Benchmark density functional theory calculations for nanoscale conductance

M. Strange,[a] I. S. Kristensen, K. S. Thygesen, and K. W. Jacobsen
Center for Atomic-scale Materials Design, Department of Physics, Technical University of Denmark, DK-2800 Kgs. Lyngby, Denmark

(Received 26 September 2007; accepted 8 January 2008; published online 20 March 2008)

We present a set of benchmark calculations for the Kohn-Sham elastic transmission function of five representative single-molecule junctions. The transmission functions are calculated using two different density functional theory methods, namely an ultrasoft pseudopotential plane-wave code in combination with maximally localized Wannier functions and the norm-conserving pseudopotential code SIESTA which applies an atomic orbital basis set. All calculations have been converged with respect to the supercell size and the number of $\mathbf{k}_{\parallel}$ points in the surface plane. For all systems we find that the SIESTA transmission functions converge toward the plane-wave result as the SIESTA basis is enlarged. Overall, we find that an atomic basis with double zeta and polarization is sufficient (and in some cases, even necessary) to ensure quantitative agreement with the plane-wave calculation. We observe a systematic downshift of the SIESTA transmission functions relative to the plane-wave results. The effect diminishes as the atomic orbital basis is enlarged; however, the convergence can be rather slow. © *2008 American Institute of Physics*. [DOI: 10.1063/1.2839275]

I. INTRODUCTION

First-principles calculations of electrical conductance in nanoscale contacts represent a main challenge in computational nanophysics. The interest for this type of calculations began in the mid-1990s, where advances in experimental techniques made it possible to contact individual molecules, thereby making it possible to study the transport of electrons through true nanoscale structures.[1,2] Apart from the scientific interest, the development of reliable simulation tools for nanoscale quantum transport is relevant not only in relation to the continued miniaturization of conventional semiconductor electronics but also for the introduction of a new generation of molecule based electronics.

It has by now become standard to calculate conductance in nanoscale contacts by employing a combination of nonequilibrium Green's function theory (NEGF) and ground state density functional theory (DFT). The resulting NEGF-DFT formalism provides a numerically efficient way of evaluating the Landauer-Büttiker conductance due to electrons moving in the effective Kohn-Sham (KS) potential without having to calculate the scattering states explicitly. It has been applied extensively to a number of different systems ranging from pure metallic contacts, over organic molecules, to carbon nanotubes suspended between metallic electrodes. Overall, the approach has been successful in describing qualitative features and trends;[3,4] however, quantitative agreement with experiments has mainly been obtained for strongly coupled systems such as metallic point contacts, monatomic chains, as well as junctions containing small chemisorbed molecules.[5–7]

It is generally accepted that the NEGF-DFT method only provides an approximation to the true conductance—even if the exact exchange-correlation (xc-)functional could be used, and the quality of the result is expected to be strongly system dependent. Moreover, it is not easy to estimate the effect of using approximate xc functionals such as the local-density approximation (LDA) or generalized gradient approximation (GGA). We mention here that more sophisticated methods for quantum transport based on configuration interaction, the GW method, time-dependent DFT, and the Kubo formula have recently been proposed.[8–12] However, these schemes are considerably more demanding than the NEGF-DFT and at present, they cannot replace NEGF-DFT in practical applications.

Irrespective of the validity of the NEGF-DFT approach and the role played by the approximate functionals, it remains important to establish a general consensus concerning the exact result of a NEGF-DFT calculation for a given xc functional and specified system geometry, i.e., a benchmark. Although this might seem trivial, the present situation is rather unsatisfactory as different results have been published by different groups for the same or very similar systems (several examples will be given in the text). Perhaps, the best example is provided by benzene dithiolate between gold contacts where the calculated conductance varies with up to two orders of magnitude for similar geometries.[3,13–18]

The relatively large variation of the results indicates that the conductance, or more generally, the elastic transmission function, is a highly sensitive quantity. Indeed, the implementation of the open boundary conditions defining the scattering problem represents some numerical challenges. Small errors in the description of the coupling between the finite scattering region and the infinite leads as well as improper *k*-point samplings in supercell approaches can introduce significant errors in the resulting transmission function.

[a]Electronic mail: strange@fysik.dtu.dk.

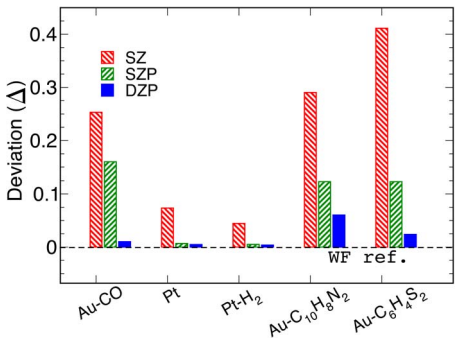

FIG. 1. (Color online) Deviation between the WF and SIESTA transmission functions for the five reference systems studied. The dashed line indicates zero deviation from the WF transmission. Notice that the SIESTA results converge toward the WF result as the PAO basis is enlarged.

In this paper, we take a first step toward establishing a common reference for NEGF-DFT calculations by performing benchmark calculations for a set of five representative nanoscale contacts. The benchmarking is achieved by comparing the transmission function obtained using two different and independent, albeit similar, NEGF-DFT methods: In one case, the Hamiltonian is obtained from the SIESTA DFT program which uses a basis of localized pseudoatomic orbitals (PAOs) together with norm-conserving pseudopotentials. The second method applies a basis of maximally localized Wannier functions (WFs) obtained from the DACAPO DFT code which uses plane waves and ultrasoft pseudopotentials. In both cases, we use periodic boundary conditions in the directions perpendicular to the transport direction and we apply the PBE xc functional.[19]

The five reference systems we have chosen for our benchmark study are (i) a monoatomic gold chain with a single CO molecule adsorbed, (ii) a three-atom Pt chain suspended between Pt electrodes, (iii) an H_2 molecule bridging two Pt electrodes, (iv) benzene-dithiolate (BDT) between Au electrodes, and (v) bipyridine between Au electrodes. The systems have been chosen according to the criterion that both experimental data as well as previous NEGF-DFT calculations are available in the literature. Furthermore, they are representative in the sense that they cover a broad class of systems: Homogeneous and heterogeneous, computationally simple (one dimensional) and more complex, and strongly as well as weakly coupled.

A main result of our work is summarized in Fig. 1 where we show the overall deviation,

$$\Delta = \frac{1}{E_0 - E_1} \int_{\varepsilon_F + E_1}^{\varepsilon_F + E_0} |T_{\mathrm{WF}}(\varepsilon) - T_{\mathrm{PAO}}(\varepsilon)| \mathrm{d}\varepsilon, \tag{1}$$

between the transmission functions calculated using the WF and PAO basis sets, respectively. The energy E_1 is taken as the lowest lying band edge in the lead, while the cutoff energy E_0 is taken to be the energy above which the WFs are no longer able to reproduce the exact KS eigenstates of the system which is typically ~3 eV above the Fermi level. For all the systems, we find that the deviation Δ decreases as the SIESTA basis is enlarged, meaning that the SIESTA transmission functions converge toward the WF result. We take this as evidence for the correctness of the WF results and the justification for the use of the term *benchmark* calculation.

In general, we find that the double-zeta polarized (DZP) basis provides very good agreement with the WF basis, whereas the single-ZP (SZP) and, in particular, the SZ basis can produce substantially incorrect features in the transmission function.

The paper is organized as follows. In Sec. II, we briefly review the NEGF-DFT formalism and introduce the two specific implementations used in the present study. In Secs. III–VI, we present the benchmark calculations for the five reference systems, and in Sec. VIII, we give our conclusions.

II. METHOD

In this section, we first outline the NEGF-DFT method which has become standard for nanoscale conductance calculations. The two specific NEGF-DFT implementations applied in the present work are then introduced and their key parameters are discussed. We then consider the important issue, common to both methods, of how to treat periodic boundary conditions in the plane perpendicular to the transport direction. We end the section with a discussion of the advantages and disadvantages of the two methods.

A. NEGF-DFT

The zero temperature, linear response conductance due to noninteracting electrons scattering off a central region (C) connected to thermal reservoirs via two ballistic leads (L and R) can be written as

$$G = G_0 T(\varepsilon_F), \tag{2}$$

where $T(\varepsilon)$ is the elastic transmission function and $G_0 = 2e^2/h$ is the quantum unit of conductance. Using the NEGF formalism, Meir and Wingreen have derived a very useful formula which expresses the transmission function in terms of the Green's function of the central region,[20]

$$T(\varepsilon) = \mathrm{Tr}[G^r(\varepsilon)\Gamma_L(\varepsilon)G^a(\varepsilon)\Gamma_R(\varepsilon)]. \tag{3}$$

In this expression, the trace runs over the central region basis functions and $\Gamma_{L/R}$ is obtained from the lead self-energies [defined in Eq. (5) below] as $\Gamma_{L/R} = i(\Sigma_{L/R} - \Sigma_{L/R}^\dagger)$.

In the NEGF DFT method, both the leads and central region are modeled by the effective KS Hamiltonian, $\hat{h}_{\mathrm{KS}} = \frac{1}{2}\nabla^2 + v_{\mathrm{eff}}(\mathbf{r})$. The self-consistent effective potential consists of the well-known parts $v_{\mathrm{eff}} = v_{\mathrm{ext}} + v_H + v_{\mathrm{xc}}$. Introducing a basis of localized orbitals, $\{\phi_i\}$, we define the Hamiltonian and overlap matrices by $H_{ij} = \langle \phi_i | \hat{h}_{\mathrm{KS}} | \phi_j \rangle$ and $S_{ij} = \langle \phi_i | \phi_j \rangle$, respectively. In the original derivation by Meir and Wingreen, the basis was assumed to be orthogonal, but the generalization to nonorthogonal basis sets shows that Eq. (3) still holds when the Green's function is defined as[21]

$$G(z) = [zS_C - H_C - \Sigma_L(z) - \Sigma_R(z)]^{-1}. \tag{4}$$

Here, the matrices H_C and S_C are the blocks of H and S corresponding to the central region basis functions. The retarded Green's function $G^r(\varepsilon)$ is obtained for $z = \varepsilon + i0^+$, and the advanced Green's function is obtained for $z = \varepsilon - i0^+$ or $G^a = (G^r)^\dagger$.

The self-energy of lead α is given by

$$\Sigma_\alpha(z) = (zS_{C\alpha} - H_{C\alpha})g^0_\alpha(z)(zS_{\alpha C} - H_{\alpha C}), \quad (5)$$

where $H_{C\alpha}$ and $S_{C\alpha}$ are the coupling and overlap matrices between basis functions in the central region and lead α, respectively. g^0_α is the surface Green's function describing the isolated semi-infinite lead, $g^0_\alpha(z)=[zS_\alpha - H_\alpha]^{-1}$, which can be calculated recursively using the decimation technique.[22] We have used a finite value for the positive infinitesimal 0^+ in the leads and in the central region of 10^{-1} and 10^{-3} eV, respectively. By using a relatively large infinitesimal in the lead, we obtain a considerably speedup due to faster convergence of the recursive calculation of the surface Green's function. We checked that a smaller value does not change our results.

B. Method 1: Wannier functions from plane-wave DFT

In method 1, the Kohn-Sham Hamiltonian is obtained from an accurate plane-wave pseudopotential DFT code.[23] The ion cores are replaced by ultrasoft pseudopotentials,[24] and we use an energy cutoff of 25 Ry for the plane-wave expansion. The Kohn-Sham eigenstates are transformed into partly occupied WFs,[25] which are used to obtain a tight-binding-like representation of the Hamiltonian. The WFs are constructed such that any eigenstate below a selected energy E_0 can be exactly represented by a linear combination of WFs. In the applications, we have chosen E_0 in the range of 2–4 eV above the Fermi level. In this way, the accuracy of the plane-wave calculation is carried over to the WF basis for all energies relevant for transport.

By performing separate DFT calculations for the (periodic) leads and C, we obtain a set of WFs for each region. Note that C always contains a few buffer layers of the lead material on both sides of the nanocontact to ensure that the KS potential at the end planes of C has converged to its value in the leads. Since the WFs in the lead, in general, will differ from those in the outermost lead unit cells of the central region, care must be taken to evaluate the coupling and overlap matrices $H_{C\alpha}$ and $S_{C\alpha}$. Notice also that although the WFs by construction are orthogonal within each region, WFs belonging to different regions will, in general, be nonorthogonal. For more details on the construction of the WFs and the calculations of the Hamiltonian matrix for the combined L-C-R system, we refer to Ref. 26. We shall refer to the results obtained from method 1 as the WF results.

C. Method 2: PAO SIESTA basis

Method 2, is based on the DFT code SIESTA,[27] which uses finite range PAOs (Ref. 28) as basis functions and Troullier-Martins norm-conserving pseudopotentials.[29] As in method 1, the Hamiltonians for the leads and the central region are obtained from separate calculations. Because the KS potentials to the left and right of C, by definition have converged to the value in the leads, we can take the coupling between central region and lead α, $H_{C\alpha}$, from the pure lead calculation. Note that this is in contrast to method 1, where the different shapes of the WFs in the periodic lead and the lead part of the central region make it essential to evaluate the coupling matrix directly. Note also that this approximation, i.e. the use of the intralead coupling matrix elements ($H_{\alpha\alpha}$) in $H_{C\alpha}$, can be controlled by including a larger portion of the lead in C. In practice, we find that three to four atomic layers must be included in C on both sides of the junction to obtain converged conductances.

In the present study, we restrict ourself to the standard PAOs for SIESTA: SZ, SZP, and DZP. For the confinement energy, determining the range of PAOs, we use 0.01 Ry, and for the mesh cutoff, we use 200 Ry.

D. Common ingredients

In both methods 1 and 2, we treat exchange and correlation effects with the PBE energy functional.[19] Furthermore, we impose periodic boundary conditions in the surface plane directions. This means that we are, in fact, considering the conductance of a periodic array of junctions instead of just a single junction. Instead of the localized basis function $\phi_n(\mathbf{r})$ (this could be a WF or a PAO), we thus consider the Bloch function

$$\chi_{n\mathbf{k}_\parallel} = \sum_{\mathbf{R}_\parallel} e^{i\mathbf{k}_\parallel \cdot \mathbf{R}_\parallel} \phi_n(\mathbf{r} - \mathbf{R}_\parallel), \quad (6)$$

where $\mathbf{R}_\parallel$ runs over supercells in the surface plane and $\mathbf{k}_\parallel$ is a wave vector in the corresponding two-dimensional Brillouin zone (BZ). Since $\mathbf{k}_\parallel$ is a good quantum number, we can construct the Hamiltonian, $H(\mathbf{k}_\parallel)$, for each $\mathbf{k}$ point separately. This, in turn, implies that the conductance *per* junction is given by the average

$$G = \sum_{\mathbf{k}_\parallel} w(\mathbf{k}_\parallel) G(\mathbf{k}_\parallel), \quad (7)$$

where $w(\mathbf{k}_\parallel)$ are symmetry determined weight factors. Unless stated otherwise, we have used a 4×4 Monkhorst-Pack $\mathbf{k}_\parallel$-point sampling of the surface BZ, which for all the systems studied yields conductances converged to within a few percent.[26,30] We take the Fermi level of the bulk lead as the common Fermi level of the combined system by shifting the levels in the central region by a constant. This is done by adding to H_C the matrix δS_c, where $\delta=[H_L]_{0,0}-[H_C]_{0,0}$ and the (0,0) element corresponds to the on-site energy of a basis function located near the interface between L and C.

The main advantages of method 1 are the following: (i) The accuracy of the plane-wave calculation carries over to the WF basis set. (ii) The WF basis set is truly minimal and often results in even fewer basis functions than a SZ basis. The WF basis, thus, combines high accuracy with high efficiency. The price that one has to pay is that the actual construction of well localized WFs is not always straightforward and requires some user interaction, in particular, for metallic systems. Also, the lack of finite support of the WFs is unwanted in the context of transport; although in practice, it is not a serious problem since the WFs are well localized. Finally, as already explained above, the risk of obtaining different WFs for two similar but nonidentical systems renders it less straightforward to patch the parts together using the Hamiltonians obtained for the separate calculations.

Most of the disadvantages of the WF basis are resolved by the PAO basis set: By construction, they have finite sup-

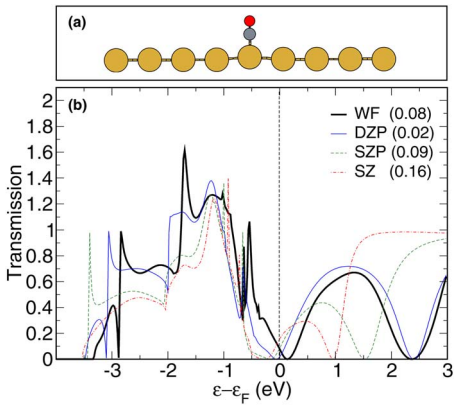

FIG. 2. (Color online) (a) Central region used to describe a single CO molecule adsorbed on a monatomic Au wire. (b) Transmission functions for the Au wire CO system calculated using method 1 (WF) and method 2 for three different PAO basis sets. The transmission function at the Fermi level is indicated in the parentheses following the legends.

port and are identical as long as the atomic species on which they are located are the same. This renders it straightforward to patch together Hamiltonians for separate subsystems as long as the KS potential can be smoothly matched at the interfaces. On the other hand, to obtain an accuracy matching the WFs, one needs to use a significantly larger number of orbitals and, thus, longer computation times as compared to the WF method.

III. GOLD CHAIN WITH CO

In this section, we calculate the conductance of an infinite gold chain with a single CO molecule adsorbed. Scanning tunneling microscope (STM) experiments suggest that CO strongly depresses the transport of electrons through gold wires.[31] This has been supported by NEGF-DFT calculations[32] which show that the transmission function indeed drops to zero at the Fermi level. The use of infinite gold chains as leads is clearly an oversimplification of the real situation; however, the model seems to capture the essential physics, i.e., the suppression of the conductance, and furthermore, is well suited as a benchmark system due to its simplicity.

The geometry of the system is shown in Fig. 2(a). We use a supercell with transverse dimensions of 12×12 Å^2 and take all bond lengths from Ref. 32: $d_{\mathrm{Au-Au}}=2.9$ Å, $d_{\mathrm{Au-C}}=1.96$ Å, and $d_{\mathrm{C-O}}=1.15$ Å. The Au atom holding the CO is shifted toward CO by 0.2 Å. In method 1, we obtain six WFs per Au atom and seven WFs for the CO molecular states. Due to the elongated bond length of the Au wire, we found it necessary in method 2 to increase the range of the Au PAOs in order to converge the band structure of the Au wire. The confinement energy was, therefore, in this case set to 10^{-4} Ry.

In Fig. 2(b), we show the calculated transmission function using three different PAO basis sets and the WF basis set. Overall, the PAO result approaches the WF result as the basis set is enlarged. For the largest PAO basis (DZP), the agreement is, in fact, very satisfactory given the differences in the underlying DFT methods, e.g., ultrasoft versus norm-conserving pseudopotentials. The remaining difference can be further reduced by a rigid shift of the DZP transmission by about 0.15 eV.

All transmission functions feature an antiresonance near the Fermi level. However, upon enlarging the PAO basis, the position of the antiresonance shifts as follows: −0.27 (SZ), −0.16 (SZP), −0.06 (DZP), and 0.12 eV (WF). Note that the position of the antiresonance obtained with the WFs is approached as the PAO basis set is increased. Also, the curvature of the antiresonance is improved as the PAO basis set is enlarged. The improvements in these features are, however, not directly reflected in the conductances indicated in the parentheses following the legends in Fig. 2(b). The reason for this apparent disagreement is the rigid shift between the PAO and WF transmission functions.

We observe that our results differ from the calculation in Ref. 32: While the latter finds two peaks in the energy range of 0–2 eV, our converged transmission function shows a single broad peak. In general, both our PAO and WF based transmission functions present less structure than the transmission function reported in Ref. 32. We suspect that these differences are related to the way the coupling $H_{\alpha C}$ is calculated in Ref. 32.

IV. Pt CONTACT

Atomic point contacts formed from late transition metals such as Au, Pt, and Pd show very stable and reproducible features in conductance measurements.[1] This, together with the simplicity implied by their homogeneity, makes them ideal as benchmark systems for transport calculations. Here, we consider the conductance of a pure Pt contact for which both experimental conductance data[33–36] as well as theoretical calculations[5,7,37] are available.

Conductance histograms obtained from mechanically controlled break junction experiments on pure Pt samples show a peak near $1.5G_0$, indicating that as a Pt contact is pulled, structures with a conductance at around $1.5G_0$ are frequently formed. NEGF-DFT calculations have shown that (zigzag) monatomic Pt chains indeed have a conductance close to this value.[5,7,36] Moreover, the calculations predict an increasing conductance as the Pt chain is stretched and evolves from a zigzag to a linear configuration. This effect has also been observed experimentally.[35]

In Fig. 3(a), we show the supercell used to model the scattering region of the Pt contact. The Pt contact is modeled by two four-atom pyramids attached to (111) surfaces containing 3×3 atoms in the surface plane. In order to ensure that the effective KS potential has converged to its bulk value at the end planes of the supercell, we include three to four atomic layers (*ABC-CABC* stacking) on either side of the pyramids. The chain is formed by inserting a single Pt atom between the apex atoms of the two pyramids. We have relaxed the contact region (pyramids+chain) while keeping the rest of the structure fixed in the bulk configuration with lattice constant of 3.93 Å and a distance of 14.60 Å between the (111) surfaces. The cutoff energy used in the construction of WFs was set to $\varepsilon_F+4.0$ eV ensuring that the KS eigenstates below this value are exactly reproducible in terms of

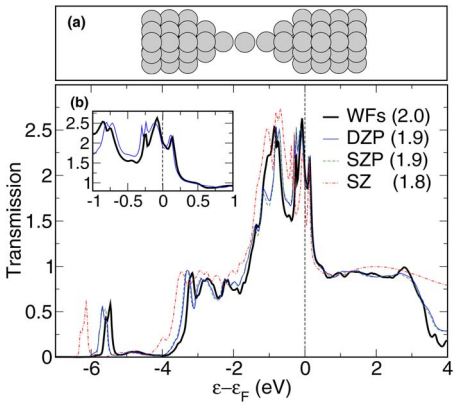

FIG. 3. (Color online) (a) Supercell used for the DFT calculation of a short linear Pt chain between Pt(111) surfaces. (b) The calculated transmission function using methods 1 and 2. The transmission at the Fermi level is indicated in the parentheses following the legends. In the inset, we show the transmission function in the important region near the Fermi level for the DZP basis set and the WF basis set.

the WFs. The transmission function was converged by a 4×4 $\mathbf{k}_{\|}$-point sampling as stated in Sec. II D.

In Fig. 3(b), we show the calculated transmission functions using methods 1 and 2. The qualitative agreement between the two methods is striking; however, only the SZP and DZP basis sets provide quantitative agreement with the WF result. The SZ basis set results in a downshift of the peak at −6 eV and an incorrect description of the features in the important region near the Fermi level. Here, the converged transmission function shows two peaks positioned at ε_F −0.8 eV and just below the Fermi level, respectively. The main peak astride the Fermi level, in fact, consists of three smaller peaks, as seen more clearly in the inset for the DZP and WF basis sets. These particular features in the transmission function were also observed in Ref. 37 for a similar Pt contact, employing a method based on quantum chemistry software and a description of the bulk electrodes by a semiempirical tight-binding Hamiltonian on a Bethe lattice.[38] Also, the calculated conductance of $2.3G_0$ is in agreement with our results, considering the structural differences.

In Fig. 4, we show the calculated conductance of the Pt contact for three electrode displacements. The three configurations correspond to an unstrained Pt chain, the chain just before it snaps, and the broken chain, respectively. The surface-surface distances are 13.62, 14.60, and 14.75 Å in the three cases.

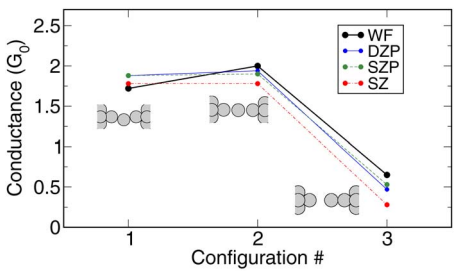

FIG. 4. (Color online) Conductance for three different configurations during the stretching of a small Pt chain. Configurations 1, 2, and 3 correspond to the unstrained chain, maximally strained chain, and a broken chain, respectively. The contact atoms are shown in the insets.

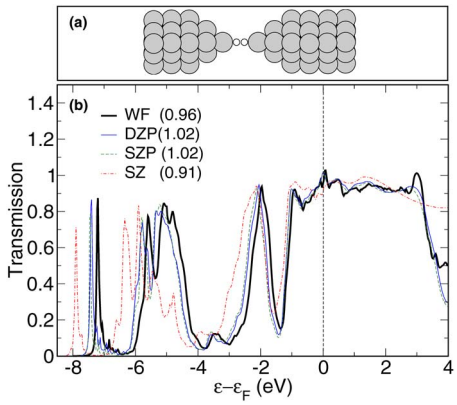

FIG. 5. (Color online) (a) Supercell used to model the central region of the Pt–H_2–Pt junction. (b) Transmission function for the Pt-hydrogen bridge. The transmission function at the Fermi level is indicated in the parentheses following the legends.

All basis sets, except for the SZ, are able to reproduce the trend of increasing conductance prior to rupture. The SZ basis set underestimates the absolute conductance by nearly $0.5G_0$ in the strained and broken configurations as compared to the WF result. The conductance calculated with the SZP and DZP basis sets is almost identical and shows results more consistent with the WF basis for all three configurations.

V. Pt–H_2–Pt CONTACT

In this section, we consider the simplest possible molecular junctions, namely, a single hydrogen molecule between metallic Pt contacts. Similar to the metallic point contacts, the Pt–H_2–Pt junction shows stable and reproducible behavior in conductance measurements. In particular, a very pronounced peak close to $1G_0$ appears in the conductance histogram obtained when a Pt contact is broken in a hydrogen atmosphere.[33] Although reported conductance calculations show significant variation (see below), there have been given substantial evidence that the structure responsible for the peak consists of a single hydrogen molecule bridging the Pt contacts.[33,39]

Several groups have published NEGF-DFT calculations for the transmission function of the Pt–H_2–Pt system. Most find a conductance of $(0.9-1.0)G_0$,[4,6,33,41] but also much lower values of $(0.2-0.5)G_0$ have been reported in Ref. 40.

For the benchmark calculations, we use the same setup as in Sec. IV with the central Pt atom replaced by a hydrogen molecule [see Fig. 5(a)]. The relevant bond lengths determining the structure after relaxation of the Pt pyramids and the hydrogen atoms are $d_{\mathrm{Pt-H}}=1.7$ Å and $d_{\mathrm{H-H}}=1.0$ Å.

In Fig. 5(b), we show the calculated transmission functions. Similar to the case of the Pt contact, the agreement between the different calculations is striking, especially in the important region around the Fermi level. The SZ basis set reproduces the qualitative features of the larger basis sets but introduces a considerable downshift of the low-lying peaks.

The very good agreement between the two methods indicates that the transmission function for this system is rather insensitive to the basis set. We stress, however, that a proper $\mathbf{k}_{\|}$-point sampling of the transmission function is crucial to

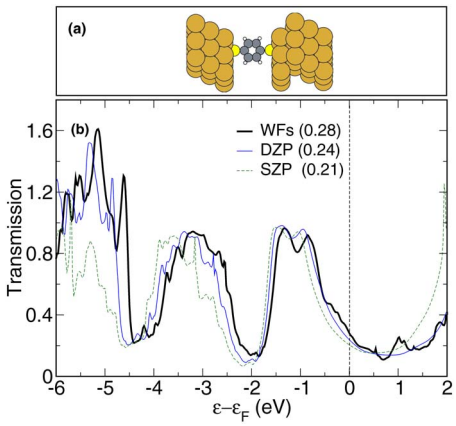

FIG. 6. (Color online) (a) Supercell used to model the central region of the Au(111)–BDT–Au(111) system with S at the fcc hollow site. (b) The calculated transmission functions. Note, that the SZ transmission function has been omitted for clarity. The transmission function at the Fermi level is indicated in the parentheses following the legends.

obtain meaningful results independently of the quality of the basis set. Restricting the calculation to the Γ point yields a transmission function with a (unphysical) peak at the Fermi level.[6] We note in passing that such a peak is present in the transmission function reported in Ref. 4. Such unphysical features resulting from an insufficient $\mathbf{k}_\parallel$-point sampling are not properties of the molecular junction but are rather due to van Hove singularities in the quasi-one-dimensional leads.[30] The results reported in Ref. 41 are based on SIESTA DFT code and show good agreement with our results. The conductance obtained in one of the early theoretical calculations[40] on the hydrogen molecular bridge is considerably lower than our and most other results. The calculational method applied in Ref. 40 is, however, the same as applied in the study of pure Pt contacts,[37] which agrees well with our results as discussed in Sec. IV. We speculate if this could be related to the smaller size of the Pt cluster used to model the electrodes in Ref. 40 as compared to the one used in Ref. 37. Another possibility for the discrepancies is the use of the B3LYP energy functional in Ref. 40 instead of a LDA/GGA functional used in most other works.

VI. BENZENE-1,4-DITHIOL BETWEEN Au(111) SURFACES

The BDT molecule suspended between gold electrodes was among the first single-molecule junctions to be studied and has become the standard reference for calculations of nanoscale conductance. Depending on the experimental setup, measured conductances vary between $10^{-4}G_0$ and $10^{-1}G_0$,[42–46] while the calculated values typically lie in the range of $(0.05–0.4)G_0$.[3,13,16–18,47–49] In general, it has been found that the transmission function is strongly dependent on the bonding site of the S atom,[18,48] while variations in the Au–S bond length only affects the transmission function weakly.[47]

As our objective is to establish a computational benchmark for the Au-BDT system, we choose the simple junction geometry, shown in Fig. 6(a). The S atoms are placed at the minimum energy positions in the fcc hollow sites of the Au(111) surface and the molecule has been relaxed while keeping the Au atoms fixed in the bulk crystal structure. We use a Au lattice constant of 4.18 Å and a distance between the Au(111) surfaces of 9.68 Å. With these constrains the relevant bond lengths are $d_{\mathrm{Au–S}}=2.45$ Å, $d_{\mathrm{S–C}}=1.73$ Å, and $d_{\mathrm{C–H}}=1.09$ Å.

In Fig. 6(b), we show the calculated transmission functions (the SZ result has been omitted for clarity). Notice that we plot the transmission function only up to 2 eV above the Fermi level. This is because the WF transmission at larger energies is sensitive to the parameters used in the construction of the WFs, in particular, the cutoff energy E_0, and thus, we cannot be sure about the WF result above 2 eV$+\varepsilon_F$.

The three transmission functions agree very well in the energy range from 2 eV below the Fermi level to 1 eV above the Fermi level, while only the DZP result agrees quantitatively with the WF result in the entire energy range. We again notice the downshift of the PAO transmission functions relative to the WF result.

The presence of a broad transmission peak positioned at ~1 eV below the Fermi level is in qualitative agreement with previous results.[3,16,47,48,50,51] For more stretched configurations, i.e., for larger values of the S–C bond length, than the one used in the present study, the broad peak splits into two more narrow peaks.[26]

The transmission function presented in Ref. 3 was obtained using a method very similar to our method 2; however, the reported conductance of $0.4G_0$ is almost twice as high as our DZP results of $0.24G_0$. The large conductance arises because the transmission peak closest to the Fermi level is considerably broader than what we find. If, however, we restrict the $\mathbf{k}_\parallel$ to the Γ point, we find the same broadening as in Ref. 3 and a very similar conductance of $0.37G_0$. Another feature of the Γ-point only transmission function is that the second peak positioned at ~3 eV below the Fermi level separates into a number of more narrow peaks.

In Ref. 16, the transmission function is calculated from the linear combination of muffin-tin orbitals–atomic sphere approximation method and averaged over 36 irreducible $\mathbf{k}_\parallel$ points. Both the width and the position of the two peaks in the transmission function at 1 and 3 eV below the Fermi level are in good agreement with our results. The height of the former peak is, however, lower than in our calculation and this reduces the conductance to a value of $0.07G_0$. We suspect that this difference could be due to differences in the adopted contact geometries.

When comparing a supercell approach to quantum transport with a cluster based calculation as the one in Ref. 47, it is essential that (i) the cluster size is converged and (ii) the number of $\mathbf{k}_\parallel$ points and supercell size are converged. In the supercell approach, a $N\times N$ Monkhorst-Pack sampling of the surface Brillouin zone corresponds to a Γ-point calculation for a supercell consisting of the original supercell repeated $N\times N$ in the surface plane.[25]

Extrapolating our converged calculations for 3×3 atoms within the surface plane of the supercell and 4×4 $\mathbf{k}_\parallel$ point to a Γ-point calculation gives a supercell consisting of ~1000 atoms. We speculate that clusters of similar sizes are needed to reach the same level of convergence. However, the re-

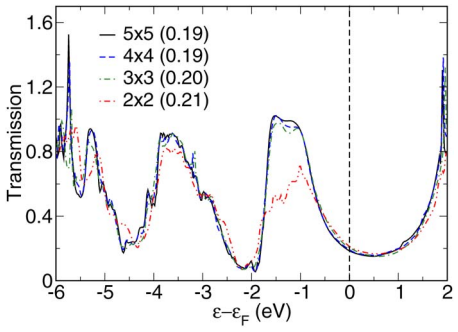

FIG. 7. (Color online) The transmission function of Au(111)–BDT–Au(111) for supercells containing a single BDT molecule and with the number of Au(111) surface atoms varying from 2×2 to 5×5 atoms, as indicated in the legends. All the calculations apply the SZP basis set and have been converged with respect to the number of $\mathbf{k}_\parallel$ points. The transmission function at the Fermi level is indicated in the parentheses following the legends.

peated supercell introduces a periodic array of molecules on the surface, which could give rise to interference effects blurring the comparison to single-molecule cluster calculations. To quantify this intermolecule interference effect, we show in Fig. 7 the SZP transmission function for the Au(111)–BDT–Au(111) system, where the number of Au atoms in the surface plane is varied from 2×2 to 5×5 atoms. Each calculation has been converged with respect to the number of $\mathbf{k}_\parallel$ points by a 4×4 Monkhorst-Pack sampling for all the supercells, except the smallest supercell for which 8×8 $\mathbf{k}_\parallel$ points was needed.

It is evident that the transmission function is well converged with 3×3 atoms in the surface plane. This shows that our calculations should be directly comparable to fully converged single-molecule cluster calculations.

VII. BIPYRIDINE BETWEEN Au(111) SURFACES

As the last reference system, we consider a bipyridine molecule attached between two gold electrodes. STM experiments on bipyridine molecules in a toluene solution[52] show that the conductance of Au-bipyridine junctions is quantized in multiples of $0.01G_0$ which was interpreted as the formation of stable contacts containing one or more molecules. The conductance is expected to be sensitive to the details of the contact geometry;[53] however, for the benchmark calculation, we use a flat Au(111) surface with bipyridine binding at an on-top site which is the minimum energy configuration, as shown in Fig. 8(a). The Au electrodes are the same as used for the BDT molecule in Sec. VI. The Au(111)–N distance is 2.180 Å, while the distance between the Au(111) surfaces is 11.53 Å.

The transmission functions calculated using either PAOs or WFs are shown in Fig. 8(b). At first, it is noted that the overall structures of the transmission functions are similar. We have used a logarithmic scale to make the differences in the low transmission regime more visible. In the SIESTA calculations, the position of the narrow lowest unoccupied molecular orbital (LUMO) peak which governs the transport is underestimated but converges toward the WF result as the PAO basis set is enlarged [see the inset of Fig. 8(b)]. The alignment of the LUMO energy level with respect to the

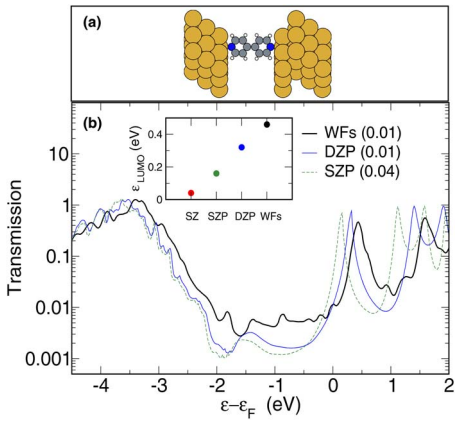

FIG. 8. (Color online) (a) Supercell used to describe the central region of the bipyridine-Au(111) junction. (b) Calculated transmission functions (the SZ result has been omitted for clarity). The inset shows the dependence of the LUMO position on the basis sets. The transmission function at the Fermi level is indicated in the parentheses following the legends.

Fermi level and its relation to charge transfer were studied in Ref. 54. The LUMO peak is close to the Fermi level and in this regime, it is expected that small changes in the position of the LUMO peak should change the conductance considerably. However, this is not the case when comparing the DZP basis set to the WF basis set since the conductance is, in fact, unchanged even though the position of the LUMO peak differs. The reason is that the WF transmission function has a different tail in the high barrier tunneling regime. The origin of this difference can be twofold: (i) The density of states of the Au(111) surface which influence the LUMO's density of states could be different in the two cases. (ii) Although the WFs have rapidly decaying tails, they do not vanish and, therefore, they must be truncated. This truncation could introduce artificial features in the transmission function in the low tunneling regime.

Several groups have investigated the transport properties of bipyridine-gold junctions, and there is general agreement that the low bias conductance depends crucially on the details of the contact geometry. As different groups have chosen different geometries and models for the gold electrodes, a direct comparison of the reported transmission functions is difficult.

To the best of our knowledge, the first theoretical paper on the bipyridine system is by Tada *et al.*[55] In their calculations, bipyridine is adsorbed on top of a Au atom of a rather small Au cluster, and the coupling to the infinite electrodes is modeled by a broadening parameter fitted to experimental data. The zero-voltage transmission function contains some of the same peak structures as we observe. Hou *et al.*[56] have published several papers on the gold-bipyridine junction. Similar to Tada *et al.*, they include only a few gold atoms in the *ab initio* calculation and treat the coupling to electrodes through a model self-energy term. The peak structure of the transmission function is quite different from ours. This could be due to the small size of the gold clusters used to mimic the electrodes. While most other groups observe tunneling through the LUMO tail,[53,54,57] Hou *et al.* argue that the transport is mainly taking place via the highest occupied MO–2 state. Calculations by Wu and co-workers[58,59] obtained using

a SIESTA-based transport code,[60] for bipyridine attached to the on-top site of a gold surface show overall good agreement with our results [see Fig. 7(a) in Ref. 58]. The minor differences are probably related to the fact that only the Γ point has been used in the latter paper.

VIII. CONCLUSIONS

We have established a set of benchmark calculations for the Kohn-Sham (PBE) elastic transmission function of five representative single-molecule junctions using two different methods based on independent DFT codes: (i) A plane-wave DFT code in combination with maximally localized Wannier functions. (ii) The SIESTA program which applies finite range pseudoatomic orbitals.

For all five systems, we find that the SIESTA result converges toward the WF result as the SIESTA basis is enlarged from SZ to DZP with the latter yielding very good quantitative agreement with the WF transmission. In the SIESTA calculations, the transmission peaks relative to the peaks obtained with the plane-wave calculation are systematically shifted toward lower energies. The problem can be overcome by enlarging the SIESTA basis; however, the convergence can be rather slow.

ACKNOWLEDGMENTS

The authors acknowledge support from the Danish Center for Scientific Computing through Grant No. HDW-1103-06. The Center for Atomic-Scale Materials Design is sponsored by the Lundbeck Foundation.

[1] N. Agrait, A. L. Yeyati, and J. M. van Ruitenbeek, Phys. Rep. **377**, 81 (2003), and references therein.
[2] A. Nitzan and M. A. Ratner, Science **300**, 1384 (2003).
[3] K. Stokbro, J. Taylor, M. Brandbyge, J.-L. Mozos, and P. Ordejón, Comput. Mater. Sci. **27**, 151 (2003).
[4] J. C. Cuevas, J. Heurich, F. Pauly, W. Wenzel, and G. Schön, Nanotechnology **14**, R29 (2003).
[5] V. M. García-Suárez, A. R. Rocha, S. W. Bailey, C. J. Lambert, S. Sanvito, and J. Ferrer, Phys. Rev. Lett. **95**, 256804 (2005).
[6] K. S. Thygesen and K. W. Jacobsen, Phys. Rev. Lett. **94**, 036807 (2005).
[7] M. Strange, K. S. Thygesen, and K. W. Jacobsen, Phys. Rev. B **73**, 125424 (2006).
[8] P. Delaney and J. C. Greer, Phys. Rev. Lett. **93**, 036805 (2004).
[9] K. S. Thygesen and A. Rubio, J. Chem. Phys. **126**, 091101 (2007).
[10] P. Darancet, A. Ferretti, D. Mayou, and V. Olevano, Phys. Rev. B **75**, 075102 (2007).
[11] S. Kurth, G. Stefanucci, C.-O. Almbladh, A. Rubio, and E. K. Gross, Phys. Rev. B **72**, 035308 (2005).
[12] P. Bokes and R. W. Godby, Phys. Rev. B **69**, 245420 (2004).
[13] M. Di Ventra, S. T. Pantelides, and N. D. Lang, Phys. Rev. Lett. **84**, 979 (2000).
[14] D. Q. Andrews, R. Cohen, R. P. Van Duyne, and M. A. Ratner, J. Chem. Phys. **125**, 174718 (2006).
[15] C. Toher and S. Sanvito, Phys. Rev. Lett. **98**, 056801 (2007).
[16] S. V. Faleev, F. Léonard, D. A. Stewart, and M. van Schilfgaarde, Phys. Rev. B **71**, 195422 (2005).
[17] K. Varga and S. T. Pantelides, Phys. Rev. Lett. **98**, 076804 (2007).
[18] J. Tomfohr and O. F. Sankey, J. Chem. Phys. **120**, 1542 (2004).
[19] P. Perdew, K. Burke, and M. Ernzerhof, Phys. Rev. Lett. **77**, 3865 (1996).
[20] Y. Meir and N. S. Wingreen, Phys. Rev. Lett. **65**, 2512 (1992).
[21] K. S. Thygesen, Phys. Rev. B **73**, 035309 (2006).
[22] F. Guinea, C. Tejedor, F. Flores, and E. Louis, Phys. Rev. B **28**, 4397 (1983).
[23] B. Hammer, L. B. Hansen, and J. K. Nørskov, Phys. Rev. B **59**, 7413 (1999); S. R. Bahn and K. W. Jacobsen, Rep. Sci. Res. Inst. **4**, 56 (2002); The DACAPO code can be downloaded at http://www.camp.dtu.dk/software.
[24] D. Vanderbilt, Phys. Rev. B **41**, 7892 (1990).
[25] K. S. Thygesen, L. B. Hansen, and K. W. Jacobsen, Phys. Rev. Lett. **94**, 026405 (2005); Phys. Rev. B **72**, 125119 (2005).
[26] K. S. Thygesen and K. W. Jacobsen, Chem. Phys. **319**, 111 (2005).
[27] J. M. Soler, E. Artacho, J. D. Gale, A. García, J. Junquera, P. Ordejón, and D. Sanchez-Portal, J. Phys.: Condens. Matter **14**, 2745 (2002).
[28] E. Artacho, D. Sánchez-Portal, P. Ordejón, A. García, and J. M. Soler, Phys. Status Solidi B **215**, 809 (1999).
[29] N. Troullier and J. L. Martins, Solid State Commun. **74**, 613 (1990).
[30] K. S. Thygesen and K. W. Jacobsen, Phys. Rev. B **72**, 033401 (2005).
[31] N. Nilius, T. M. Wallis, and W. Ho, Phys. Rev. Lett. **90**, 186102 (2003).
[32] A. Calzolari, C. Cavazzoni, and M. B. Nardelli, Phys. Rev. Lett. **93**, 096404 (2004).
[33] R. H. M. Smit, Y. Noat, C. Untiedt, N. D. Lang, M. C. van Hemert, and J. M. van Ruitenbeek, Nature (London) **419**, 906 (2002).
[34] C. Untiedt, D. M. Dekker, D. Djukic, and J. M. van Ruitenbeek, Phys. Rev. B **69**, 081401 (2004).
[35] J. M. Krans, C. J. Muller, I. K. Yanson, Th. C. M. Govaert, R. Hesper, and J. M. van Ruitenbeek, Phys. Rev. B **48**, 14721 (1993).
[36] S. K. Nielsen, Y. Noat, M. Brandbyge, R. H. M. Smit, K. Hansen, L. Y. Chen, A. I. Yanson, F. Besenbacher, and J. M. van Ruitenbeek, Phys. Rev. B **67**, 245411 (2003).
[37] J. Fernández-Rossier, D. Jacob, C. Untiedt, and J. J. Palacios, Phys. Rev. B **72**, 224418 (2005).
[38] J. J. Palacios, A. J. Pérez-Jiménez, E. Louis, and J. A. Vergés, Phys. Rev. B **64**, 115411 (2001).
[39] D. Djukic, K. S. Thygesen, C. Untiedt, R. H. M. Smit, K. W. Jacobsen, and J. M. van Ruitenbeek, Phys. Rev. B **71**, R161402 (2005).
[40] V. M. García-Suárez, A. R. Rocha, S. W. Bailey, C. J. Lambert, S. Sanvito, and J. Ferrer, Phys. Rev. B **72**, 045437 (2005).
[41] Y. García, J. J. Palacios, E. SanFabián, J. A. Vergés, A. J. Pérez-Jiménez, and E. Louis, Phys. Rev. B **69**, R041402 (2004).
[42] M. A. Reed, C. Zhou, C. J. Muller, T. P. Burgin, and J. M. Tour, Science **278**, 252 (1997).
[43] M. Tsutsui, Y. Teramae, S. Kurokawa, and A. Sakai, Appl. Phys. Lett. **89**, 163111 (2006).
[44] X. Xiao, B. Xu, and N. J. Tao, Nano Lett. **4**, 267 (2004).
[45] J. Ulrich, D. Esrail, W. Pontius, L. Venkataraman, D. Millar, and L. H. Doerrer, J. Phys. Chem. B **110**, 2462 (2006).
[46] S. Ghosh, H. Halimun, A. K. Mahapatro, J. Choi, S. Lodha, and D. Janes, Appl. Phys. Lett. **87**, 233509 (2005).
[47] F. Evers, F. Weigend, and M. Koentopp, Phys. Rev. B **69**, 235411 (2004).
[48] H. Kondo, H. Kino, J. Nara, T. Ozaki, and T. Ohno, Phys. Rev. B **73**, 235323 (2006).
[49] E. G. Emberly and G. Kirczenow, Phys. Rev. Lett. **91**, 188301 (2003).
[50] S.-H. Ke, H. U. Baranger, and W. Yang, J. Chem. Phys. **127**, 144107 (2007).
[51] Y. Xue, S. Datta, and M. A. Ratner, J. Chem. Phys. **115**, 4292 (2001).
[52] B. Xu and N. J. Tao, Science **301**, 1221 (2003).
[53] R. Stadler, K. S. Thygesen, and K. W. Jacobsen, Phys. Rev. B **72**, R241401 (2005).
[54] R. Stadler and K. W. Jacobsen, Phys. Rev. B **74**, 161405 (2006).
[55] T. Tada, M. Kondo, and K. Yoshizawa, J. Chem. Phys. **121**, 8050 (2004).
[56] S. Hou, J. Zhang, R. Li, J. Ning, R. Han, Z. Shen, X. Zhao, Z. Xue, and Q. Wu, Nanotechnology **16**, 239 (2005); S. Hou, J. Ning, Z. Shen, X. Zhao, and Z. Xue, Chem. Phys. **327**, 1 (2006); R. Li, S. Hou, J. Zhang, Z. Qian, Z. Shen, and X. Zhao, J. Chem. Phys. **125**, 194113 (2006).
[57] A. J. Perez–Jimenez, J. Phys. Chem. B **109**, 10052 (2005).
[58] X. Wu, Q. Li, J. Huang, and J. Yang, J. Chem. Phys. **123**, 184712 (2005).
[59] Q. Li, X. Wu, J. Huang, and J. Yang, Ultramicroscopy **105**, 293 (2005).
[60] M. Brandbyge, J. L. Mozos, P. Ordejón, and K. Stokbro, Phys. Rev. B **65**, 165401 (2002).